Magnetic Resonance Imaging 60 (2019) 76–84

Contents lists available at ScienceDirect

Magnetic Resonance Imaging

journal homepage: www.elsevier.com/locate/mri

Original Contribution

MRI-based texture analysis of the primary tumor for pre-treatment prediction of bone metastases in prostate cancer

Yueren Wang[a], Bing Yu[a], Fei Zhong[b], Qiyong Guo[a,*], Kexin Li[a], Yang Hou[a], Nan Lin[a]

[a] Department of Radiology, Shengjing Hospital of China Medical University, Shenyang, Liaoning, PR China
[b] Institute of Big Data Technology, BOCO, Beijing, PR China

ARTICLE INFO

Keywords:
Prostate cancer
Bone metastases
Magnetic resonance imaging
Intratumor heterogeneity
Radiomics

ABSTRACT

Purpose: To identify texture features of multiparametric MRI (mp-MRI) for pre-treatment prediction of bone metastases (BM) in patients with prostate cancer (PCa).

Patients and methods: One-hundred and seventy-six patients with clinicopathologically confirmed PCa were enrolled , and the data was gathered from January 2008 to January 2018. A total of 976 texture features were extracted from T2-weighted (T2-w) and dynamic contrast-enhanced T1-weighted (DCE T1-w) MRI. Step regression, ridge regression and LASSO regression method model was applied to select features and develop the predicting model for BM. The performance of the radiomics features, PSA level and Gleason Score were explored with the respect to the receiver operating characteristics (ROC) curve. Multivariable logistic regression analysis starting with the following clinical risk factors (PSA level, Gleason Score and age) and imaging biomarkers were applied to develop diagnostic model for BM in PCa.

Results: The texture features, which consisted of 15 selected features, were significantly associated with BM ($P < 0.01$). The combined MRI features derived from T2-w and DCE T1-w showed better prognostic performance (AUC = 0.898) than features derived from single sequence (T2WI AUC = 0.875, DCE T1-w AUC = 0.870) and Gleason Score (AUC = 0.731) for pre-treatment prediction of BM in PCa. MRI -based imaging biomarker combined with clinical risk factors (free PSA, age and Gleason score) yielded the highest AUC(AUC = 0.916). Multivariate regression analysis showed that the imaging biomarker was an independent risk factor for the detection of bone metastases along with f-PSA level (free PSA) and Gleason score.

Conclusion: Multiparametric MRI-based texture feature was significant predictor for BM in PCa. Clinical risk factors combined with MRI-based texture feature could further improve the prediction performance, which provide an illustrative example of precision medicine and may affect treatment strategies.

1. Introduction

Prostate cancer (PCa) is the most prevalent male malignancy in the western world, with > 1 in 7 men expected to be diagnosed with the disease in their lifetime, and approximately 27,500 deaths every year are attributed to this disease in the United States alone [1,2]. In recent years, the incidence of PCa has been growing every year in China. The main causes of treatment failure are biochemical recurrences and distant metastases. Bone is the most frequent site of metastases in PCa. Although the type and incidence of bone metastases (BM) may vary between primary tumor sites, they all have a significant clinical impact, inducing serious consequences on patients' quality of life. Skeletal related events (SREs) represent the most clinically important complications of BM and include pathological fractures, spinal cord injury, hypercalcemia and pain requiring surgical intervention or radiotherapy [3]. These risk groups are heterogeneous in terms of radiosensitivity, rendering it important to identify other predictors of recurrence to intensify local or systemic treatments for tumors with poor prognosis [4]. Therefore, pretreatment identification of distant metastases in patients with advanced PCa is crucial to identify the prognosis and make decisions regarding treatment [5]. Unfortunately, there is no systematic study to verify the predictive factors that might accurately predict BM in patients with PCa.

With the development of the prostate imaging report and data system (PI-RADS) and the rapid development of radiomics based on big data and artificial intelligence, multiparametric magnetic resonance imaging (mp-MRI) has become the best noninvasive modality in the diagnosis of prostate disease. It is of great value in the early stage of

* Corresponding author at: Department of Radiology, Shengjing Hospital of China Medical University, Sanhao Street No36, Heping District, Shenyang, Liaoning 110004, PR China.
E-mail address: guoqy@sj-hospital.org (Q. Guo).

https://doi.org/10.1016/j.mri.2019.03.007
Received 1 November 2018; Received in revised form 7 March 2019; Accepted 8 March 2019

prostate cancer with accurate diagnosis, treatment options, therapeutic evaluation and prognosis evaluation. Over the last few years, imaging biomarkers, popularly called radiomics, have been recognized as potentially powerful tools to aid in identifying patients with tumor subgroups with poor prognosis [4]. Texture analysis (TA), which reflect tissue heterogeneity, is related to a variety of mathematical techniques able to evaluate the grey-level intensity distribution and spatial organization in an image [6]. Among these indices, features calculated from the grey-level co-occurrence matrix (GLCM) are the most used due to their simple computation and interpretation [6]. On the GLCM, various statistics can be computed: energy, entropy, correlation, homogeneity, contrast, etc. GLCM captures the frequency of co-occurrence of similar intensity levels over the region, which describes the texture of the region of interest [2]. Recently published studies [1,2,7,8] have demonstrated that TA can distinguish or classify benign and malignant lesions in prostate, another recent focus of TA has been the assessment of therapy response in PCa [4]. However, to the best of our knowledge, no study has so far investigated the feasibility to detect cancerous lesions directly in the target tissue before they appear visible to the human reader or predict BM from the primary tumor.

In this context, the aim of this study was to determine whether texture features acquired on mp-MRI images before treatment combined with clinicopathologic risk factors can predict BM in patients with PCa.

2. Materials and methods

2.1. Study population

Our Institutional Review Board approved this retrospective study and waived the need to obtain informed consent. The entire cohort of this study was acquired from January 2008 to January 2018 records of the Institutional Picture Archiving and Communication System (PACS, Neusoft), which was used to identify patients who had histologically confirmed PCa without evidence of distant metastases at diagnosis. 176 patients were enrolled in our study, according to the inclusion criteria and exclusion criteria, the following inclusion criteria applied: histologically confirmed PCa on needle biopsy; multiparametric 3.0 T MRI, according to European Society of Urogenital Radiology recommendations, where the tumor had to be apparent; standard unenhanced and contrast-enhanced MRI performed within 2 weeks before or after the diagnosis of PCa. The exclusion criteria were: patients were diagnosed to have other primary cancer; presence of post-biopsy hemorrhage on MRI; radical prostatectomy (RP), androgen deprivation therapy (ADT), radiotherapy (RT), chemotherapy (CT) before MRI; and follow-up period $<$ 24 months in the BM-negative cohort. A flow chart of the study is presented in Fig. 1a. All the patients underwent a total of 12 transrectal biopsies that can be divided into six biopsies in each lobe.

The clinicopathologic characteristics of these patients in the training and validation dataset are listed in Table 1. The patients were identified and divided into two cohorts at a ratio of 3:1 using computer generated random numbers. 132 patients were allocated to the training cohort, while 44 patients were allocated to the independent validation cohort. There was no difference between the training and the validation cohort in the clinicopathologic characteristics. The data combined imaging biomarker and clinicopathologic characteristics were tested in the validation cohort.

2.2. Follow-up and endpoint

The study cohort can be considered as “watchful waiting” patient group due to their age and other conditions. Patients were followed up by means of clinical examination and PSA level analysis every 1–3 months. After a median follow-up of 42 months (range: 7–119 months), follow-up is terminated when bone metastases occur as the endpoint. Finally, 91 patients exhibited BM, defined according to ECT. Patients were monitored with frequent laboratory tests, including prostate specific antigen (PSA) level, testosterone level, and regular imaging, which included bone scan and computed tomography or magnetic resonance imaging of the chest, abdomen and pelvis every 8 weeks during the first 6 months then every 12 weeks thereafter [9].

2.3. MRI technique

MRI scan was performed using two different 3.0 T scanners (Ingenia, Philips Healthcare, The Netherlands; Signa HDxt, GE Healthcare, USA), both with 16-channel phased-array surface coils, with the patients scanned in supine position. MRI sequences included axial turbo spin echo T2-w and axial dynamic contrast-enhanced (DCE) T1-w. Dynamic MRI of the prostate was carried out using a fixed time-delay method. After the precontrast series, gadopentetate dimeglumine was injected within 10 s. Postcontrast series were obtained 20, 50, 80 and 110 s after the initiation of contrast-agent injection. The sequences' parameters are detailed in Table 2.

2.4. Image post-processing and texture analysis

Only axial T2-w and DCE T1-w Digital Imaging and Communications in Medicine (DICOM) images were considered. The study workflow can be divided into three steps: manual segmentations, and feature extraction. All manual segmentations of the tumor were performed by a radiologist (with 7 years of experience: YR.W.) and each segmentation was validated by a senior radiologist with 19 years of experience, mainly in genitourinary cancers (N.L.). The region of interest (ROI) around the tumor outline for the largest cross-sectional area was delineated on both the axial T2-w and DCE T1-w (post contrast 50 s) images with the help of available MRI images (including T1-w, diffusion-weighted, ADC), MRI radiology reports, and pathology biopsy. The ROIs were re-binned to 16 Gy-level histogram bins between the minimum and maximum intensity limits. We used IBEX software for segmentation and textural analysis (open source, http://bit.ly/IBEX_MDAnderson).

In total, 976 features were ultimately extracted from the tumor ROIs in the axial T2-w images and DCE T1-w images, including 6 kinds of features: shape, intensity, intensity histogram, GLCM, grey level run length matrix (GLRLM), and neighbor intensity difference. These texture features are typically categorized into first and second order features, based on the method applied to estimate how the pixels are interrelated. First order features are solely based on intensity values and the shape of the ROI. These features are extracted either directly or from a histogram analysis prior to any mathematical transformation and regardless of spatial configuration. Intensity-based features such as variance and entropy address the overall dispersion of grey levels but given their nature, are limited regarding precise spatial distribution of grey levels within the tumor [10,11]. To quantify intratumoral heterogeneity incorporating spatial information, TA was applied which constitutes the second-order statistical output. These entail approaches like GLCM and GLRLM, as well as neighbor intensity difference [10,11]. Haralick textural features consisted of a specific relation of pixels with their local neighborhood [4,7],were derived from GLCM. In our study, a total of 330 Haralick features were extracted, including: cluster prominence, cluster shade, cluster tendency, contrast, correlation, dissimilarity, inverse variance, energy, entropy, and so forth. A grey level run is a set of consecutive, collinear picture points having the same grey level value [12], grey level run length (GLRL) is defined as the number of contiguous voxels that have the same grey level value and it characterizes the GLRLs of different grey level intensities in any direction [12,13]. In this study, we extracted 33 GLRLM features. Histogram is the grey level function, describes the grey level image with the number of pixels, normally refers to a histogram of the pixel intensity values. Neighbor Intensity Difference consists of busyness, coarseness, complexity, contrast and texture strength.

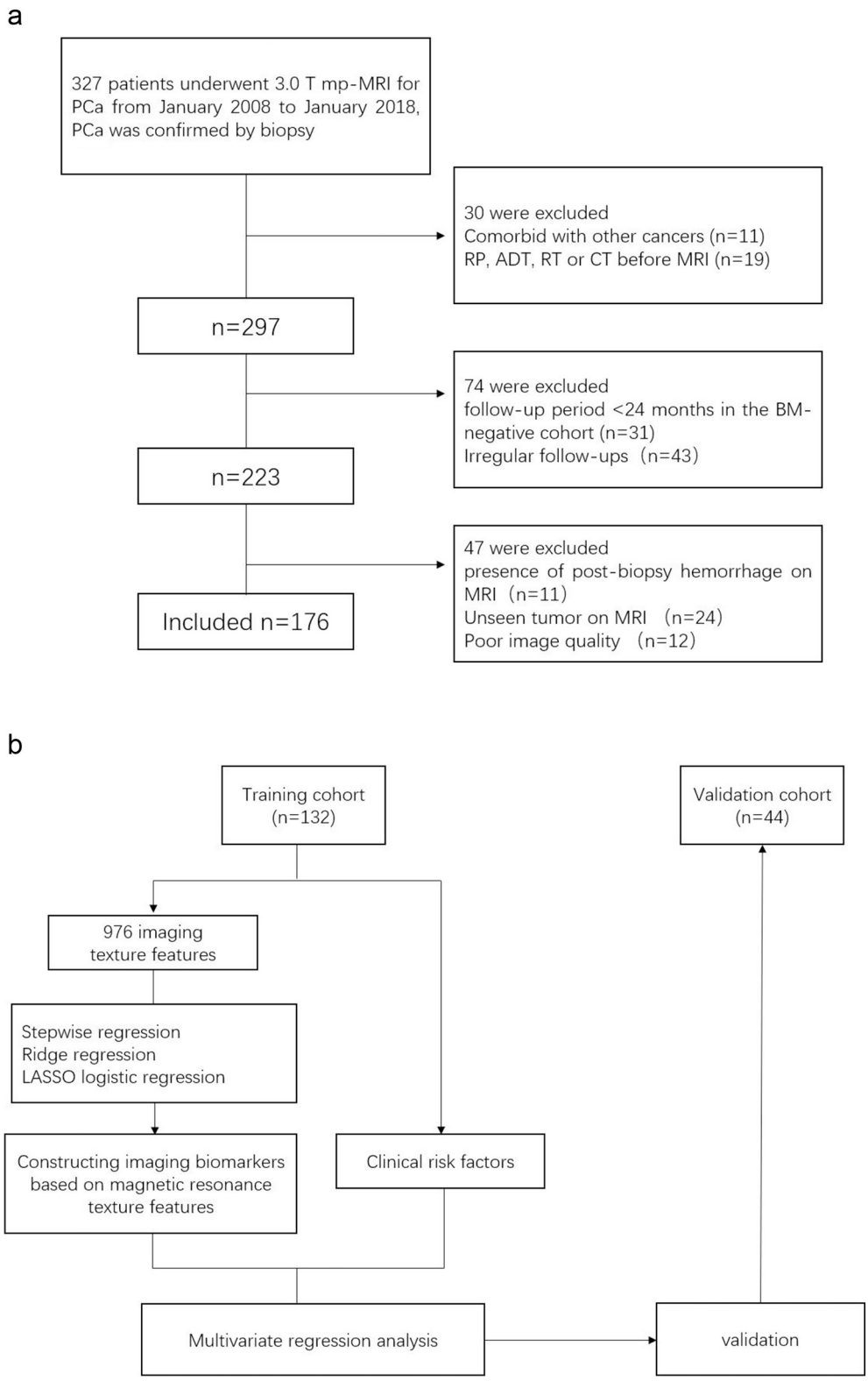

Fig. 1. Flow chart of the study. RP, radical prostatectomy; ADT, androgen deprivation therapy; RT, radiotherapy; CT, chemotherapy.

2.5. Radiomics feature extraction/selection and radiomics signature construction

Linear regression, ridge regression and logistic regression model was applied to select features and develop the predicting model for BM. A formula was generated using a linear combination of selected features that were weighted by their respective LASSO coefficients; the tuning parameter λ was selected in the LASSO model via 10-fold cross validation based on minimum criteria; the formula was then used to calculate a risk score (defined as the radiomics score). Risk score for each patient reflect the risk of BM.

Table 1
Patient characteristics in primary and validation cohorts.

	Training cohort			Validation cohort		
	BM(+)	BM(−)	P	BM(+)	BM(−)	P
Age(years)						
Age(median)	70	71	0.316	73	68	0.092
Age(range)	49–86	53–86		49–85	53–78	
PSA level(ng/ml)						
Mean ± SD						
t-PSA	86.9 ± 120.9	40.1 ± 34.4	0.056	75.9 ± 29.5	48.1 ± 36.5	0.068
f-PSA	24.2 ± 19.4	6.00 ± 7.50	< 0.001	31.1 ± 19.6	7.51 ± 10.5	< 0.001
Gleason score						
7	34	32		10	8	
8	9	18		6	7	
9	18	15		7	5	
10	6	0		1	0	
Total	67	65		24	20	

Table 2
MRI sequence parameters.

	Philips Ingenia	GE Signa HDXT
Sequence parameter	n = 168	n = 8
T2-weighted imaging		
Sequence type	SPAIR	FSE
TR (msec)	2057–4352	2180–5240
TE (msec)	65–120	116–126
Field of view(mm)*	250	340
matrix	432 × 432	512 × 512
Section thickness(mm)	4.53	4.53
Flip angle(degrees)	90	90
Dynamic Contrast-enhanced imaging		
Sequence type	THRIVE	LAVA-XV + C
TR (msec)	3.74–5.3	2.69–4.4
TE (msec)	0.00–2.6	1.18–1.5
Field of view(mm)*	300	420
matrix	336 × 336	512 × 512
Section thickness(mm)	3	3

2.6. Evaluation of the performance of imaging biomarker for Prediction of BM in PCa

The difference in risk scores between the BM-positive and BM-negative patients was assessed using independent *t*-test or Mann-Whitney *U* test. The predictive accuracy of the texture features was explored with the respect to the receiver operating characteristics (ROC) curve (AUC) in both the training and validation cohorts. Z test was used to compare AUC and to compute standard deviations (SD) and the 95% confidence intervals (CI). P value < 0.05 was considered statistically significant.

2.7. Validation of the performance of imaging biomarker for Prediction of BM in PCa

Multivariate regression analysis starting with the following clinical risk factors (age; PSA level; Gleason score) and imaging biomarkers was applied to develop a diagnostic model for the BM.

2.8. Statistical analysis

The LASSO logistic regression model was used with penalty parameter tuning that was conducted by 10-fold cross-validation based on minimum criteria. The likelihood ratio test with backward step-down selection was applied to the multivariate logistic regression model. Detailed descriptions of the LASSO algorithm are provided in the Supplementary Data.

ALL statistical tests were performed with R software version 3.5.1 (R Core Team. R: A language and environment for statistical computing. R Foundation for Statistical Computing, Vienna, Austria; http://www.R-project.org) and MedCalc (version 15.2.2, MedCalc Software bvba, Ostend, Belgium).

Radiomics workflow of the study is presented in Fig. 1b.

3. Results

3.1. Patient characteristics

Patient characteristics in the training and validation cohorts are given in Table 1. There were no significant differences between the two cohorts in BM prevalence. BM positivity was 50.8% and 54.5% in the training and validation cohorts, respectively. Although there was a temporal disconnect, there were no significant differences in the clinicopathologic characteristics between the primary and the validation cohort, either within the BM-positive cohort or in the BM-negative cohort, which justified their use as training and validation cohorts. There was no significant difference in the age and total PSA (t-PSA) level between the BM-positive and BM-negative groups.

3.2. MR radiomics feature extraction/selection

Of texture features, 976 features were reduced to 15 potential predictors on the basis of 132 patients in the training cohort with nonzero coefficients in the LASSO logistic regression model. The tuning parameter λ was selected in the LASSO model via 10-fold cross validation based on minimum criteria (Fig. 4a–d).

3.3. Imaging biomarker construction and evaluation of the performance of imaging biomarkers for prediction of BM in PCa

Imaging biomarker mathematical models based on T2-w texture features, DCE T1-w texture features, both T2-w and DCE T1-w texture features, and combined MR texture features with clinical risk factors were constructed, risk scores (defined as the radiomics scores) were calculated with the formulas. The formulas were provided in the Supplementary Data. Textural features used for imaging biomarker construction and the corresponding coefficients are described in Table 3.

There was significant difference between the BM-positive and BM-negative group in the imaging biomarker, either based on the T2-w images, DCE T1-w images, T2-w and DCE T1-w images, Gleason Score and combined MR texture features with clinical risk factors. The risk score was slightly lower for the BM-positive group in imaging biomarker based on T2-w texture features. The risk scores were significantly higher for the BM-positive group in the other biomarkers

Table 3
List of textural features used for imaging biomarker construction.

Number	Texture feature	Feature description	Corresponding coefficients for risk scores calculation formulas			
			T2-w	DCE T1-w	T2-w and DCE T1-w	Combined MR texture features and clinical risk factors
	GLRLM					
f1	Short run low grey level emphasis, SRLGLE	Measures the joint distribution of short runs and low grey level values, is expected large for the image with many short runs and lower grey level values and with greater values indicative of more fine textural structures [15]	0.026	2.89		0.0085
f2	Short run high grey level emphasis, SRHGLE	Measures the joint distribution of short runs and high grey level values		−5.80		
	GLCM					
f3	Auto correlation	Measure of linear dependency of grey levels of neighboring				
	135-1 auto correlation	pixels	1.59			
	0-7 auto correlation			−223.80		−497.80
	45-4 auto correlation					328.10
f4	Cluster prominence	Gauge the perceptual concepts of uniformity and proximity				
	90-4 cluster prominence		−0.22		−0.38	
	333-7 cluster prominence		0.13			
	0-4 cluster prominence		−0.0017			
	45-7 cluster prominence			−0.12	0.84	0.07
	-333-1 cluster prominence			0.45	0.59	−0.27
f5	Difference entropy	Measure of randomness of grey levels				
	135-4 difference entropy		15.87		52.91	
	135-7 difference entropy		−23.15			
f6	Dissimilarity	Reflects the dissimilarity of image grayscale distribution				
	-333-1 dissimilarity		4.76	−0.62		
	0-7 dissimilarity		6.07	−1.09		
	45-4 dissimilarity		−15.57			
	45-7 dissimilarity			−0.17	−12.00	2.42
	90-7 dissimilarity		7.46			
f7	Homogeneity	Reflect the texture homogeneity in images and measure the		−15.46	−12.83	
f8	Information measure of correlation 2	local variation in texture [16]			54.15	
f9	Variance	Measure of grey level distribution				
	45-1 variance		3.41		5.33	
f10	Inverse different moment	Measure the level of local homogeneity within the tumor		−7.50		
	333-4 inverse different moment	volume, calculation are based on assuming larger values for			7.91	
	90-4 inverse different moment	smaller grey-tone differences in pair elements within the			−9.84	−1.66
f11	InverseDiffMomenNorm	GLCM [17]				
	90-4 InverseDiffMomenNorm			−9.23		
	45-4 InverseDiffMomenNorm			−2.35	−5.50	−5.87
	Intensity direct	First order features extracted directly from a histogram				
f12	Local standard max	analysis based on intensity, address the overall dispersion of	−16.98			
f13	40,80,85-percentile	grey levels but given their nature	−0.0066		−12.47	−0.25
f14	0.025 quantile			0.20		
f15	Range			−0.85		

(Table 4).

ROC analysis demonstrated that the combined MRI features derived from T2-w and DCET1-w showed better prognostic performance than features derived from T2-w or DCET1-w alone, Gleason score for pre-treatment prediction of BM in PCa. MRI-based imaging biomarker combined with clinicopathologic characteristics (f-PSA, age and Gleason score) yielded the highest AUC(AUC = 0.916) (Fig. 2,Table 5). Z test was used to compare AUCs, there was statistical significance between the AUCs (with $P < 0.05$). Although a slightly higher AUC was observed for the model with clinical risk factors integrated into the imaging biomarkers, integration of the clinical risk factors into the prediction model did not show significantly improved prediction performance.

3.4. Validation of the performance of biomarker based on combined MR texture features and clinical risk factors for prediction of BM in PCa

The ROC curve of the biomarker based on combined MR texture features and clinical risk factors in the validation cohort is shown in Fig. 3. The biomarker yielded an AUC = 0.895 and showed a good agreement with the training cohort.

The prediction model after the addition of clinical risk factors is

Table 4
Risk scores based on different biomarkers.

	Training cohort				Validation
	T2	DCE-T1	T2 + DCE-T1	T2 + DCE-T1 + Clinical	
BM(+)	−477.05 ± 324.52	−24,645.68 ± 4463.81	−1634.59 ± 95.51	−34,688.58 ± 4392.89	−39,999.31 ± 4806.97
BM(−)	−461.26 ± 322.34	−50,338.51 ± 8604.87	−1981.60 ± 397.65	−83,945.19 ± 5595.25	−83,889.90 ± 4133.12
P	< 0.001	< 0.001	< 0.001	< 0.001	< 0.001

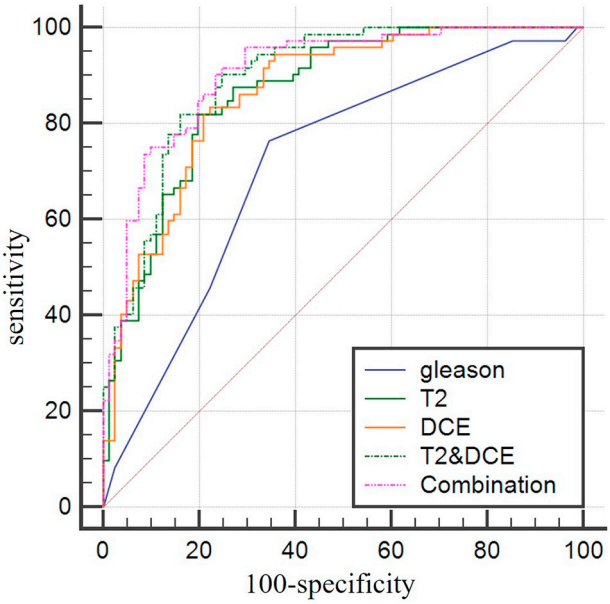

Fig. 2. show the ROC curve of the imaging biomarker based on T2-w texture features, DEC T1-w texture features, combined T2-w and DEC T1-w texture features, Gleason Score, combined MR texture features and clinical risk factors in the training cohort.

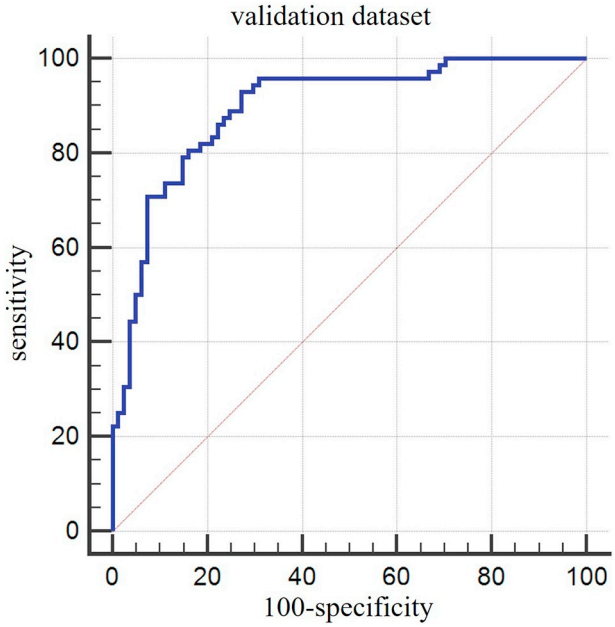

Fig. 3. ROC curve of biomarker based on combined MR texture features and clinical risk factors in the validation cohort.

shown in Table 6. Multivariate regression analysis showed that the imaging biomarker was an independent risk factor for the detection of BM, along with f-PSA level and GS.

4. Discussion

Evidence indicates that only 25% of patients with metastatic and invasive PCa live 5 years subsequent to the initial diagnosis of metastases [14]. If patients who are at high risk of metastases can be identified preoperatively, then such patients might represent an appropriate group for ADT and CT. However, the accuracy of biopsy and PSA, which is the standard clinical procedure for PCa aggressiveness, is unsatisfactory, and a considerable proportion of patients are understaged or overstaged. Thus, early accurate prediction of BM, identification of patients at high risk for BM, could allow early selection of those most likely to benefit from targeted therapy to prevent or delay BM, and/or intensive monitoring to optimize the likelihood of timely and successful intervention. MRI is a non-invasive examination and successful integration of texture-based computer-aided diagnosis tools (i.e. TA) into clinical practice could make this process quantitative and less subjective [8].

We developed and validated a diagnostic, radiomics signature–-based biomarker for the pretreatment individualized prediction of BM in patients with PCa. The model incorporating the T2-w and DCE T1-w radiomics signature that combine multiple individual texture features facilitates the pretreatment individualized prediction of BM. In this study, the T2w-based biomarker would have led to a 91.67% PPV for BM at this threshold. The combined imaging biomarker model based on T2-w and DCE T1-w texture features demonstrated adequate discrimination. The integration of imaging biomarker and traditional biochemical and pathological markers showed a slightly increase in specificity to 89.2%, with AUC = 0.916 in the training cohort, which was then surprisingly confirmed in the validation cohort. Given that BM positivity was comparable in the two cohorts, and the radiomics signature was robust for prediction and could be applied directly in the validation cohort. Thus, the noninvasive MRI-based TA, which makes use of the images we already have for free could serve as a more convenient biomarker for the prediction of BM in PCa.

For the construction of the radiomics signature, 976 candidate radiomics features were reduced to 15 kinds of potential predictors by examining the predictor-outcome association by shrinking the regression coefficients with the stepwise regression, ridge regression and LASSO regression method. Stepwise regression was used to screen for features which have significant impact on the model. Ridge regression and lasso regression were used to screen for low correlation characteristics, and we used probability density map to analyze the probability density of features and screen for distinguishing features. The texture features obtained from LASSO are generally accurate, and the regression coefficients of most features are shrunk towards zero during model fitting, making the model easier to interpret and allowing the identification of features that are most strongly associated with BM. Moreover, LASSO allows radiomics signature to be constructed by combining the selected features. We found the T2-w image-derived textural features f1, f3, f4, f5, f6, f8, f9, f12, f13 and DCE T1-w image-derived textural features f1, f2, f3, f4, f5, f6, f7, f10, f11, f14,f15

Table 5
AUC, standard deviations (SD), the 95% confidence intervals (CI), sensitivity, specificity, PPV, NPV and accuracy of the imaging biomarker for the prediction of BM in PCa patients.

	AUC	SD	95%CI	Sensitivity	Specificity	PPV	NPV	Accuracy
T2-w	0.875	0.029	0.801–0.915	0.742	0.912	0.917	0.729	0.815
DCE T1-w	0.870	0.029	0.799–0.914	0.745	0.859	0.873	0.724	0.796
T2-w + DCE T1-w	0.898	0.025	0.833–0.937	0.778	0.875	0.887	0.757	0.821
GS	0.731	0.040	0.636–0.784	0.647	0.782	0.764	0.670	0.712
T2-w + DCE T1-w + Clinical risk factors	0.916	0.024	0.847–0.946	0.806	0.892	0.885	0.817	0.849
Validation cohort	0.895	0.026	0.836–0.939	0.815	0.881	0.869	0.831	0.849

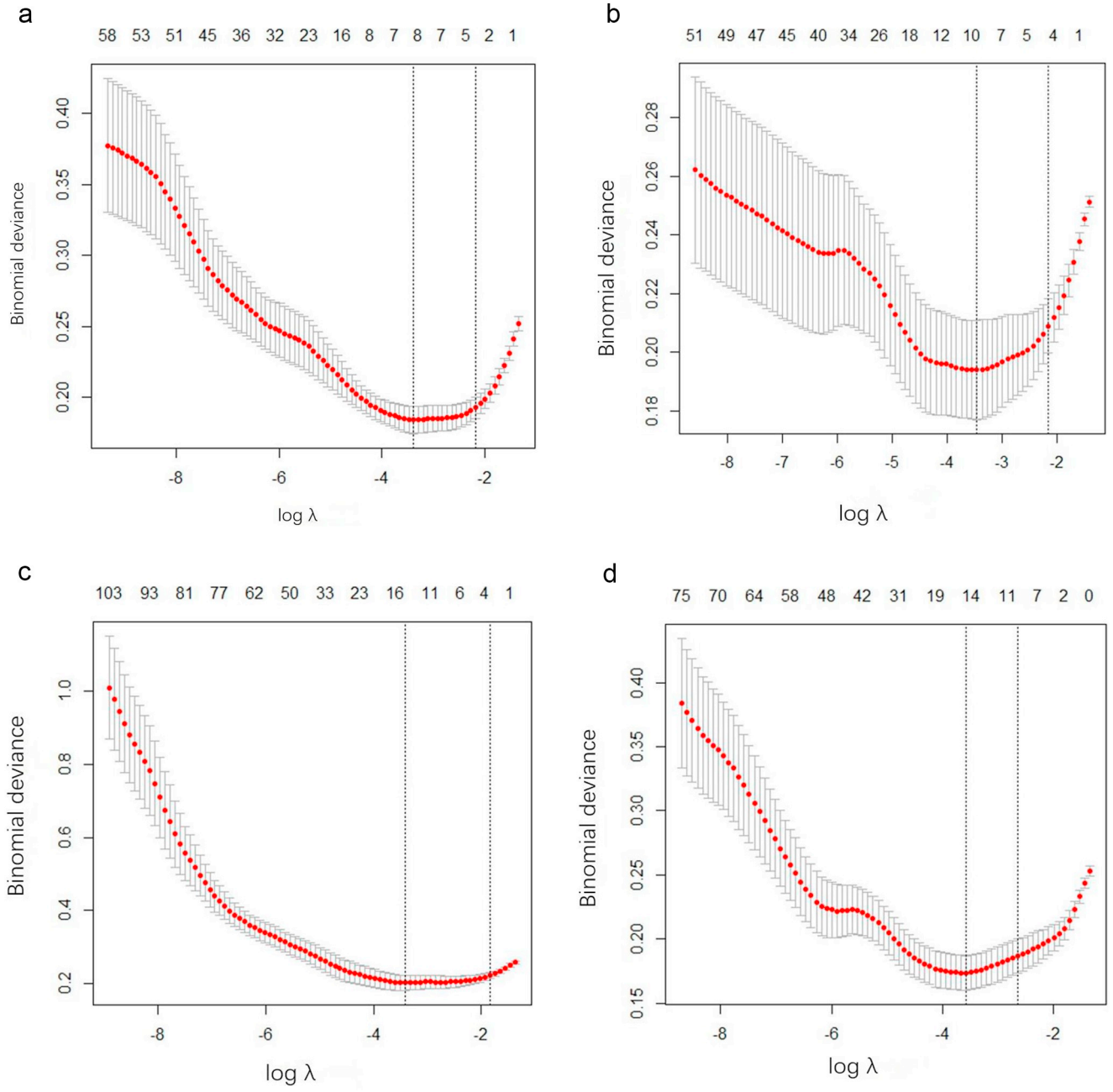

Fig. 4. Selection of the tuning parameter λ in the LASSO model via 10-fold cross validation based on minimum criteria. Binomial deviances from the LASSO regression cross-validation procedure were plotted as a function of log(λ). The y-axis indicates binomial deviances. The lower x-axis indicates the log(λ). Numbers along the upper x-axis represent the average number of predictors. Red dots indicate average deviance values for each model with a given λ, and vertical bars through the red dots show the upper and lower values of the deviances. The vertical black lines define the optimal values of λ, where the model provides its best fit to the data.
4a T2 w-based texture feature selection, the optimal λ value 0.035 was selected from T2W texture features (488 textural features).
4b DCE T1 w-based texture feature selection, the optimal λ value 0.033 was selected from DCE T1-w based texture features (488 textural features).
4c T2-w and DCE T1-w-based texture feature selection, the optimal λ value 0.034 was selected from the combined T2-w and DCE T1-w textural features(976 textural features).
4d Combined MR texture features and clinical risk factors feature selection, the optimal λ value 0.030 was selected from the combined MRI textural features (976 textural features) and clinical risk factors. (For interpretation of the references to colour in this figure legend, the reader is referred to the web version of this article.)

correlate significantly with BM, nevertheless, tumor volume was not associated with BM. Consistently significant differences were noted across all grey levels between BM-positive and BM-negative groups at both T2-w and DCE T1-w for f1, f3,f4,f5 and f6 showed higher values for prediction of BM. T2w-based f8, f9 and DCE T1 w-based f2, f7 [16], f10 [17] also showed correlation with BM, our study support the findings of Ng et al. [18] who showed that more homogeneity resulted in a poorer prognosis in malignant tumors. In our study, histogram-based features including f12–15 are solely based on intensity and the shape of the ROI, these features are extracted either directly or from a histogram analysis prior to any mathematical transformation and regardless of spatial configuration, intensity-based features address the overall dispersion of grey levels but given their nature, are limited regarding precise spatial distribution of grey levels within the lesion. [10].

The risk scores in BM-positive group are significantly higher than

Table 6
Multivariate regression analysis of clinical risk factors and imaging biomarker.

Intercept and variable	β	OR(95%CI)	P
intercept	−4952.519		< 0.001
Imaging biomarker	0.836	2.307(1.484 , 3.166)	< 0.001
f-PSA level	0.127	1.135(1.098 , 1.172)	< 0.001
Age	0.044	1.045	0.238
Gleason score	1.055	2.871(2.240 , 3.501)	< 0.001

f-PSA, free PSA.

those in BM-negative group; This trend is consistent with the findings of Anton et al.[19],suggesting an increased heterogeneity of the texture was found in BM-positive group compared to BM-negative and lesions with increased heterogeneity are more likely to have BM or have poorer prognosis in the future, which is also supported by the findings of previous studies[20–22]. Cancer growth requires formation of new blood vessels to sustain the proliferating cells, the change causes fast extravasation of injected contrast agent and thus an increase in Ktrans when compared to healthy tissues might be a possible explanation for the association with the textural features like f1 and f2 on DCE T1-w images. Our findings are important because they suggest that first-order, GLCM and GLRLM texture parameters extracted from pre-operative imaging of the primary tumor are significantly related to biological behavior for PCa. However, there is no obvious explanation at the histological level for these differences of behavior, further investigations on how texture features are associated with tumor biological behavior may help defining on the relationship between texture heterogeneity and tumor aggressiveness or poor outcome [20].

Multivariate regression analysis showed that the imaging biomarker, f-PSA level and Gleason score (GS) were independent predictors of BM in PCa. Urologists and radiation oncologists struggle with these questions as the standard clinical prognostic factors of PSA level, GS and tumor-category are insufficient for selecting an optimal patient management strategy [2].GS is probably the most powerful prognostic factor for PCa, however, in our study the accuracy of GS to predict BM in patients with PCa is unsatisfactory (AUC = 0.731) (Fig. 2). Several factors can influence the accuracy of the biopsy GS, including the PSA level, the level of pathologist expertise, the inaccuracy of positioning, the percentage of cancer cells in the biopsy sample and the number of biopsies obtained [23]. Currently, PSA level has been clinically applied as the main predictor for BM. However, using PSA level as the inclusion criteria, the latest systematic review and meta-analysis suggested the lack of a robust definition for predicting high BM risk in PCa patients [24]. Note that there was no significant correlation between t-PSA and BM(P = 0.056,0.068), which is at odds with other previous studies [25,26], nevertheless, f-PSA level was significant related to BM in PCa (P < 0.01)in our study, suggesting f-PSA as part of a risk assessment to help guide treatment decisions in patients with BM in PCa. However, further data are required to support this approach.

Study limitations include the fact that genomic characteristics were not considered currently. In recent years, increased research with gene markers, such as KLK2, KLK3, HOMER2, BMPR1B, CHRNA2, MT1H, DPP4, MYBPC1 were found to be associated with the androgen receptor-signaling in PCa, which plays an important role in the occurrence and development of PCa. TRPM8, DPP4 and GCNT1 were found to have high positive correlations with radiomic features [27–29]. Increased expression of TBX2 promotes BM and growth in the bone microenvironment through downstream regulation [14]in patients with PCa. Radiogenomics, which focuses on the relationship between imaging phenotypes and genomics, has emerged in the field of cancer research and attracted wide concern. However, though it might be an interesting attempt, it is yet to be decided whether simply building a model of the primary tumor that applies the imaging features to predict outcomes directly is preferable to radiogenomic analysis[30,31]. Second, our study lacks validation:a multicenter validation with larger sample size is needed to acquire high-level evidence for clinical application[32]. Third, tumor ROI delineation is challenging both for automatic or manual methods. In our implementation, the ROIs were drawn in the slice with the largest lesion extent on axial plane, because they were thought to better represent the tumor and included as much of the tumor as possible to account for its heterogeneity, however, we might lack the information of sagittal and coronal planes. Moreover, there is no differentiation made between peripheral and transition zone cancer.

5. Conclusion

In conclusion, this study presents radiomics model that incorporates both the MRI-based texture features of the primary tumor and clinical risk factors, which can be conveniently used to facilitate the pre-operative individualized prediction of BM in patients with PCa. These results provide an illustrative example of precision medicine and may affect treatment strategies.

Ethics approval and Informed consent.

Institutional review board approval was obtained. Informed consent was obtained from all subjects (patients) in this study. Methodology: retrospective, diagnostic study, performed at one institution.

Conflict of interest

The authors declare that they have no conflicts of interest.

Appendix A. Supplementary data

Supplementary data to this article can be found online at https://doi.org/10.1016/j.mri.2019.03.007.

References

[1] Turkbey B, Brown AM, Sankineni S, et al. Multiparametric prostate magnetic resonance imaging in the evaluation of prostate cancer. CA Cancer J Clin 2016; 66(4): 326–336.
[2] Stoyanova R, Takhar M, Tschudi Y, et al. Prostate cancer radiomics and the promise of radiogenomics. Transl Cancer Res 2016;5(4):432–47.
[3] D'Oronzo S, Brown J, Coleman R. The value of biomarkers in bone metastasis. Eur J Cancer Care 2017;26(6).
[4] Gnep K, Fargeas A, Gutiérrez-Carvajal RE, et al. Haralick textural features on T2 -weighted MRI are associated with biochemical recurrence following radiotherapy for peripheral zone prostate cancer. J Magn Reson Imaging 2017;45(1):103–17.
[5] Zhang B, Tian J, Dong D, et al. Radiomics features of multiparametric MRI as novel prognostic factors in advanced nasopharyngeal carcinoma. Clin Cancer Res 2017;23(15):4259–69.
[6] Scalco E, Rizzo G. Texture analysis of medical images for radiotherapy applications. Br J Radiol 2017;90(1070):20160642.
[7] Wibmer A, Hricak H, Gondo T, et al. Haralick texture analysis of prostate MRI: utility for differentiating non-cancerous prostate from prostate cancer and differentiating prostate cancers with different Gleason Scores. Eur Radiol 2015;25(10):2840–50.
[8] Nketiah G, Elschot M, Kim E, et al. T2-weighted MRI-derived textural features reflect prostate cancer aggressiveness: preliminary results. Eur Radiol 2017;27(7):3050–9.
[9] Bryce AH, Alumkal JJ, Armstrong A, et al. Radiographic progression with nonrising PSA in metastatic castration-resistant prostate cancer: post hoc analysis of PREVAIL. Prostate Cancer Prostatic Dis 2017;20(2):221–7.
[10] M. D. Anderson Cancer Center Head and Neck Quantitative Imaging Working Group. Investigation of radiomic signatures for local recurrence using primary tumor texture analysis in oropharyngeal head and neck cancer patients. Sci Rep 2018;8(1):1524.
[11] Haralick RM. Statistical and structural approaches to texture. Proc IEEE 1979;67:786–804.
[12] Galloway MM. Texture analysis using gray level run lengths. Comput Graphics Image Process 1975;4(2):172–9.
[13] Parekh Vishwa, Jacobs Michael A. Radiomics: a new application from established techniques. Expert Rev Precis Med Drug Dev 2016;1(2):207–26.
[14] Nandana S, Tripathi M, Duan P, et al. Bone metastasis of prostate cancer can be therapeutically targeted at the TBX2–WNT signaling axis. Cancer Res 2017; 77(6): 1331–1344.
[15] Fei Yang, John C. Ford, Nesrin Dogan, et al. Magnetic resonance imaging (MRI)-based radiomics for prostate cancer radiotherapy. Transl Androl Urol 2018; 7(3): 445–458.
[16] Pantic I, Pantic S, Basta-Jovanovic G. Gray level co-occurrence matrix texture

analysis of germinal center light zone lymphocyte nuclei: physiology viewpoint with focus on apoptosis. Microsc Microanal 2012;18(3):470–5.
[17] Baderaldeen A. Altazi, Geoffrey G. Zhang, Daniel C, et al. Reproducibility of F18-FDG PET radiomic features for different cervical tumor segmentation methods, gray-level discretization, and reconstruction algorithms. J Appl Clin Med Phys 2017; 18(6): 32–48.
[18] Ng F, Ganeshan B, Kozarski R, et al. Assessment of primary colorectal cancer heterogeneity by using whole-tumor texture analysis: contrast-enhanced CT texture as a biomarker of 5-year survival. Radiology 2013; 266(1): 177–184.
[19] Becker AS, Schneider MA, Wurnig MC, et al. Radiomics of liver MRI predict metastases in mice. Eur Radiol Exp 2018;2(1):11.
[20] Michoux N, Van den Broeck S, Lacoste L, et al. Texture analysis on MR images helps predicting non-response to NAC in breast cancer. BMC Cancer 2015;15:574.
[21] Bhooshan N, Giger ML, Jansen SA, et al. Cancerous breast lesions on dynamic contrast-enhanced MR images: computerized characterization for image-based prognostic markers. Radiology 2010;254(3):680–690.
[22] Ahmed A, Gibbs P, Pickles M, et al. Texture analysis in assessment and prediction of chemotherapy response in breast cancer. J Magn Reson Imaging 2013; 38(1): 89–101.
[23] Rapiti E, Schaffar R, Iselin C, et al. Importance and determinants of Gleason score undergrading on biopsy sample of prostate cancer in a population-based study. BMC Urol 2013;13:19.
[24] Guo X, Zhang C, Guo Q, et al. The homogeneous and heterogeneous risk factors for the morbidity and prognosis of bone metastasis in patients with prostate cancer. Cancer Manag Res 2018; 10: 1639–1646.
[25] McArthur C, McLaughlin G, Meddings RN. Changing the referral criteria for bone scan in newly diagnosed prostate cancer patients. Br J Radiol 2012;85(1012):390–4.
[26] Thurtle D, Hsu RC, Chetan M, et al. Incorporating multiparametric MRI staging and the new histological Grade Group system improves risk-stratified detection of bone metastasis in prostate cancer. Br J Cancer 2016;115(11):1285–8.
[27] Stoyanova R, Pollack A, Takhar M, et al. Association of multiparametric MRI quantitative imaging features with prostate cancer gene expression in MRI-targeted prostate biopsies. Oncotarget 2016;7(33):53362–76.
[28] Erho N, Crisan A, Vergara IA, et al. Discovery and validation of a prostate cancer genomic classifier that predicts early metastasis following radical prostatectomy. PLoS One 2013; 8(6): e66855.
[29] Penney KL, Sinnott JA, Fall K, et al. mRNA expression signature of Gleason grade predicts lethal prostate cancer. J Clin Oncol 2011; 29(17): 2391–2396.
[30] Mazurowski MA. Radiogenomics: what it is and why it is important. J Am Coll Radiol 2015;12(8):862–6.
[31] Huang YQ, Liang CH, He L, et al. Development and validation of a radiomics nomogram for preoperative prediction of lymph node metastasis in colorectal cancer. J Clin Oncol 2016;34(18):2157–64.
[32] Wu S, Zheng J, Li Y, et al. A radiomics nomogram for the preoperative prediction of lymph node metastasis in bladder cancer. Clin Cancer Res 2017;23(22):6904–11.